

Article

Effect of Mistuning and Blade Passing Frequencies on a Turbine's Integral Mode Blade Vibration Detection Using a Pulsation Probe [†]

Takashi Ando

Turbo Systems Switzerland Ltd., Bruggerstrasse 71a, 5401 Baden, Switzerland;
takashi.ando@accelleron-industries.com

[†] This selected manuscript is a slightly revised version of the ETC2023-300 meeting paper published in the Proceedings of the 15th European Turbomachinery Conference, Budapest, Hungary, 24–28 April 2023.

Abstract: For engines operating using heavy fuel oil (HFO), the nozzle rings of turbocharger turbines are prone to severe degradation because of contamination with unburned fuel deposits. This contamination may lead to increased excitation of blade resonance. A previous study provides technical guidelines on how to extract the relevant information from pulsation spectra using a single probe installed away from the turbine trailing edge and some sound experimental proofs of integral mode turbine vibration detection. These theoretical discussions only allude to the effects of mistuning and interferences due to classical blade passing frequencies on sound radiation patterns emitted by integral blade vibration modes. In this study, both effects are thoroughly discussed. Combining the knowledge of theoretical study and further experimental results, the application range of this blade vibration detection method can be remarkably extended.

Keywords: turbocharger turbine blade vibration monitoring; pulsation measurement; nozzle ring fouling; mistuning; blade passing frequencies



Citation: Ando, T. Effect of Mistuning and Blade Passing Frequencies on a Turbine's Integral Mode Blade Vibration Detection Using a Pulsation Probe. *Int. J. Turbomach. Propuls. Power* **2023**, *8*, 37. <https://doi.org/10.3390/ijtp8040037>

Academic Editor: Antoine Dazin

Received: 7 June 2023

Revised: 21 July 2023

Accepted: 21 July 2023

Published: 2 October 2023



Copyright: © 2023 by the author. Licensee MDPI, Basel, Switzerland. This article is an open access article distributed under the terms and conditions of the Creative Commons Attribution (CC BY-NC-ND) license (<https://creativecommons.org/licenses/by-nc-nd/4.0/>).

1. Introduction

A previous study [1], in addition to providing sound experimental evidence of turbocharger turbine integral mode detection using a pulsation sensor installed on the stator side away from the turbine trailing edge, also provided theoretical backgrounds, mainly based on the work conducted by [2]. During further investigations, however, it was recognized that the theories developed in the last 20 years of the 20th century, for example [2–4], handle mainly flutters in axial compressor stages and cannot apply directly to a turbocharger's turbine integral mode resonance. Under a flutter condition, due to coupling between aerodynamic disturbance and structural eigenmode, the *IBPA* (inter-blade phase angle) will tend to unify. Note that a spatial excitation force pattern covers the entire annulus, and it sweeps with a speed different from that of the rotor. Hence, the resulting resonance will become a non-integral mode. Therefore, theories at that time could have, at least provisionally, reasonably assumed a single *IBPA* over all blades.

On the other hand, in a turbocharger radial turbine stage, integral mode resonances are the main cause of an HCF (high cyclic fatigue) failure. As Figure 1 shows, especially during a low *EO* (excitation order) resonance crossing of a radial turbine stage, eigenfrequencies of the individual blades have a scatter magnitude of up to a few percent.

In a low *EO* resonance, in contrast to NR (nozzle ring) vane count-induced ($EO > 20$) higher eigenmodes, the excitation force will not be distributed equally over the circumferences but tends to concentrate at a few angular positions, such as around the turbine casing tongue or a highly clogged NR sector. To simplify the following discussion, a single dominant excitation angular position is assumed, for example, a completely clogged NR sector. With such an excitation force pattern, all low *EO* excitation force spatial phases will

be locked to the position around the clogged NR sector. When the rotor sweeps through a resonance crossing, an individual blade reacts to the angularly fixed singular excitation force by alternating the vibratory phase from 0° (same phase as excitation) to $+90^\circ$ (resonance point) and $+180^\circ$ (“+” means, in this context, a lagging phase). Due to the mistuning, the vibratory phase alternation speed range differs between blades, so the *IBPA* will vary arbitrarily between 0 and $\pm 180^\circ$ (“+” means, in this context, running in the same direction as the rotor revolution). From these considerations, at least in the case of a radial turbine stage’s low *EO* resonances, usage of the technical term “nodal diameter” is not appropriate, so discussion should be restricted only to the *IBPA*. Additionally, the same “range” of *IBPA* will not cover the entire circumference but is confined to a few blade pairs. Note that it is a rather rare case that the *IBPA* will exactly fulfil the stepwise relation, $IBPA = \frac{2\pi \cdot k}{B}$, (k : integer, a synonym of nodal diameter, and B : Blade number).

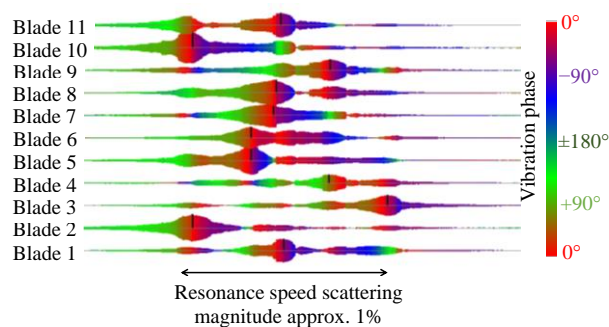


Figure 1. Response of blades in a first flap mode along excitation order six (for a radial turbine).

The first topic of the present study deals, therefore, with adaptations of the theory developed by [2] for a mistuned structure integral mode vibration with respect to the criterium of circumferential mode propagation in axial directions.

The second topic relates to interference between classical BPFs (blade passing frequencies, pulsation peaks appearing at $B \cdot n_{TC}$ and its harmonics, with B as blade count and n_{TC} as rotor revolution frequency when blades are not vibrating) and the integral mode blade vibration-originating sound radiation. The low engine order fundamental mode resonance discussed in [1] or shown in Figure 1 occurs at around 70% of maximal rotor speed, at which the blade tip velocity is well below $M = 1$ (M : Mach number). At a higher rotor speed, BPF airborne modes start to propagate undiminished in the axial direction, and pulsation amplitudes originating from BPFs will far exceed those coming from a blade vibration so that the detection of the blade vibration using a pulsation signal will become generally difficult. This study is intended to demonstrate how to handle and overcome the disadvantage of high revolution speed by analyzing experimental data in detail.

2. Theoretical Discussion

2.1. The Criterium for the Propagation of Circumferential Mode in the Axial Direction

Prior to displaying the formula for axial wave number when blades are vibrating in a not negligible bulk flow rate as formulated in [2], it is suggested first to review BPF mode axial direction propagation criteria postulated by [5]. Tyler & Sofrin formulated a simple criterium when the BPF mode, pure circumferential mode, will begin to propagate in an axial direction:

“In order that the pressure field of a spinning lobed pattern propagates in the duct (i.e., axial direction), the circumferential Mach number at which it sweeps the annulus walls must equal or exceed unity.” [5]

In other words, if there are no bulk flow disturbances over the circumference, the BPF mode can propagate in the axial direction only when the blade tip velocity equals or exceeds the sound velocity. The so-called “Tyler & Sofrin mode”, i.e., due to interactions between a bladed rotor and stator, pressure fluctuation lobe numbers other than the rotor

blade counts will arise, as discussed in the original paper, mainly in such a context that when the Tyler & Sofrin mode's lobe number is less than the rotor blade counts, because the mode sweep velocity becomes higher than the blade tip velocity, even at a lower rotor revolution speed, the BPF noise will be audible from outside.

In principle, the simple criterium, i.e., circumferential mode sweep velocity \geq sound velocity, should be applicable even when dealing with a circumferential mode originating from blade vibrations in a subsonic bulk flow rate. Now recall the axial wavenumber formula presented in [2].

$$\bar{\alpha} = \frac{U(\omega + V\bar{\beta}) \pm c_0 \sqrt{(\omega + V\bar{\beta})^2 - (c_0^2 - U^2)\bar{\beta}^2}}{c_0^2 - U^2} \tag{1}$$

$\bar{\alpha}$: Wave number in the axial direction

U : Axial bulk gas flow rate

V : Circumferential bulk gas flow rate (=blade tip velocity)

c_0 : Speed of sound

ω : Blade vibration frequency

$\bar{\beta}$: Wave number between blades in the circumferential direction, formulated as

$$\bar{\beta} = \frac{\frac{2\pi k}{B} + 2\pi m}{s} = \frac{2\pi(k + m \cdot B)}{B \cdot s} = \frac{2\pi(k + m \cdot B)}{2\pi r} \tag{2}$$

s : Spacing between two blades

k : Integer k varies between $-\frac{B}{2} \leq k \leq \frac{B}{2}$ for an even number of blades or $-\frac{B-1}{2} \leq k \leq \frac{B-1}{2}$ for an odd number of blades (synonym for nodal diameter)

m : Wave number between two blades (integer between $-\infty \dots 0 \dots +\infty$)

r : Radius of the blade tip

When the m is set, provisionally, as zero, the blade vibration frequency ω can be expressed with $\bar{\beta}$ by introducing a new term c_s , the circumferential mode sweep velocity as defined in [5]:

$$\omega = \bar{\beta} \cdot c_s \tag{3}$$

Upon inserting Equation (3) into (1), the criterion, whether a circumferential mode will propagate in the axial direction undiminished, i.e., the content of the root in (1) should be larger than zero, will become an easily comprehensible form:

$$\sqrt{(c_s + V)^2 + U^2} \geq c_0 \rightarrow \sqrt{(V \pm c_s)^2 + U^2} \geq c_0 \tag{4}$$

At this stage, it is crucially important to notice that c_s and V relate not as scalar but as vector terms. That is, the sense “ \pm ” shall be added, which is missing in the formula in [2]. However, for example, [6] put the “ \pm ” in the formula. Commonly, a frequency, i.e., oscillation cycles per time unit, is expressed as a scalar value since time has only positive values. If a point sound source is assumed, the sound will propagate in all directions so that a ω , as a point source, cannot be defined as a vector. However, as a dominant circumferential mode arises through inter-blade interactions, it can and should be treated as a vector. The value of c_s will be processed either as positive or negative, depending on the parameters in (2). So, there is no difference if “ \pm ” is explicitly put in (4). However, once this characteristic equation is expressed in the way it is in Equation (4), it becomes clear that the sense of circumferential mode sweeping direction relative to V , the rotor revolution, takes a critical role in axial direction propagation characteristics. From these considerations, it can be presumed that airborne acoustic waves released from the suction (same direction as rotor revolution) or pressure (opposite direction to rotor revolution) side of a blade should have an entirely different axial direction propagation characteristic.

Integral mode blade vibration resonance frequency relates to rotor revolution frequency and EO so that the sweep velocity c_s can be formulated as:

$$c_s = \frac{\omega}{\beta} = \frac{2\pi \cdot EO \cdot n_{TC}}{\beta} = \frac{2\pi \cdot EO \cdot n_{TC} \cdot r}{k + m \cdot B} \quad (5)$$

At a given blade vibration resonance frequency, from Equation (5), it will be clear that the highest sweep speed in favor of axial direction propagation will result when the nominator $k + m \cdot B$ takes the smallest positive value. Recalling that k can take only values in the range $-\frac{B}{2} \leq k \leq \frac{B}{2}$ for an even number of blades or $-\frac{B-1}{2} \leq k \leq \frac{B-1}{2}$ for an odd number of blades, the highest positive value of c_s is possible when $m = +1$ (if k takes a negative value) or when $m = 0$ (if k takes a positive value). This, by airborne acoustic conditions determined value, $m = 0$ or $+1$, will be commonly fulfilled in a radial turbine stage's low EO resonances, which will be demonstrated theoretically and experimentally in later chapters.

The discussion takes into account the effect of mistuning. In the introduction, it is postulated that the integral relation between the $IBPA$ and integer k does not exist in a real structure, and the $IBPA$ will not have a single value amongst the whole blade counts. To make the point clear:

$$\bar{\beta}_i = \frac{IBPA_i + 2\pi m}{s} \quad (6)$$

i : blade number, $1 \dots B$

$IBPA_i$: two-blade set vibrating with an inter-blade phase angle, $IBPA_i \leq \pm \frac{\pi}{2}$

The main difference between (2) and (6) is that in (2), each k mode is assumed to stretch over the circumference, while in (6) $IBPA_i$ will be treated sector-wise. So, the commonly applied restriction, $IBPA = \frac{2\pi k}{B}$, will not be required anymore.

In a mistuned structure, while the value of m is kept the same for all blades, the $IBPA$ varies from sector to sector. In addition, referring to Figure 1, if one of the blades crosses a resonance point, a neighboring blade does not vibrate significantly (see the response of Blades 4 and 5 or 1, 2 and 3 in Figure 1). In an extreme situation, if only one blade is vibrating, then the $IBPA$ will not be defined anymore. Conversely, an undefinable $IBPA$ can be interpreted as a configuration that contains every possible $IBPA$ value—similar to the Dirac Delta function that contains arbitrary frequencies. Refer to [7] for this basic idea.

The consequences of this theoretical consideration on blade vibration detection using pulsation sensors will be discussed in a later chapter by referring to experimental data and analysis.

2.2. Effect of Subsonic Bulk Flow on Airborne Acoustic Radiation Amplitude and Wave Number

When dealing with the turbocharger's turbine stage's airborne acoustic field characteristics, it is indispensable to take bulk flow into account because the Mach number of relative flow velocity exceeds 0.5. As displayed in Figure 2, in the case of the turbocharger's turbine stage's first flap mode, a higher magnitude of sound radiation will be released downstream than in the circumferential direction.

On the other hand, referring to [8] (pp. 721–726), amplitudes and frequencies of emitted sound at the upstream side will be amplified due to bulk flow. The amplitude amplification magnitude at neighboring blades' trailing edges amounts to approximately four times when the bulk flow Mach number is 0.74 (see Figure 3).

The circumferential modes for those axial direction propagation characteristics discussed in the previous chapter shall establish themselves in the x -axis range -1 to 0 of Figure 3. So, the sound pressure amplitude, as well as wave number, are lifted two to five times compared to those without bulk flow. Interactions between neighboring blades, enhancing or scattering depending on the $IBPA$, mainly occur at these elevated levels. Therefore, the from the blade originally emitted fraction directly downstream will play a minor role, even if the fraction of original sound radiation has higher magnitudes.

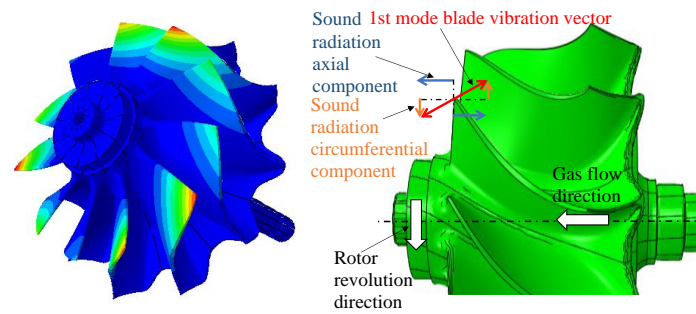


Figure 2. First flap mode shape and geometrical relation (left picture displays ND4 mode, the color indicates velocity amplitude).

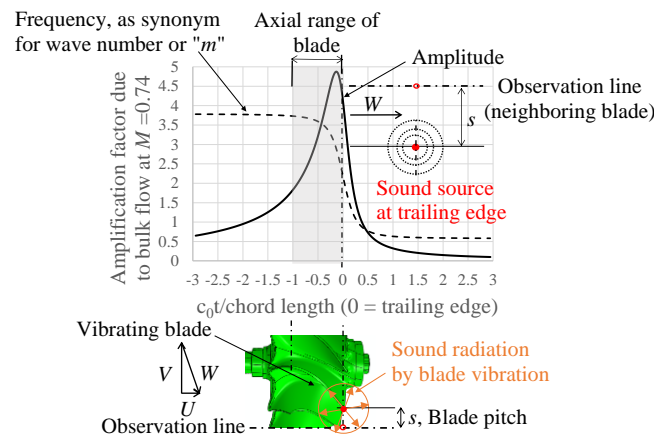


Figure 3. Emitted sound amplitude amplification behavior due to bulk flow with $M = 0.74$ (first flap mode).

Now returning to the statement about m in the last chapter, that to favour an undiminished propagation in the axial direction, m should be zero, or most preferably $+1$ (when $m = +1$, mode sweep velocity will be “added” to V , regardless of whether the *IBPA* has a positive or negative value). In the absence of bulk flow, at the first flap mode resonance condition along $EO = 6$, the wave number between two blades will amount to 0.38 , i.e., mode $m = 0$ will be dominant. However, due to bulk flow at the level of $M = 0.74$, as shown in Figure 3, the m value will be amplified by two to three times so that the actual wave number will lie between 0.76 and 1.14 in the range of the blade row i.e., mode $m = \pm 1$ will be dominant.

3. Experimental Results and Discussion

Concerning the experimental setup, refer to [1]. A piezoresistive pulsation sensor was placed approximately 1.5 times of the blade chord length away from the trailing edge on the downstream side. Eight optical sensors for BTT (blade tip timing) were distributed near the blade trailing edge.

Figure 4 displays BTT measurements and an LSMF (least squares model fit) analysis result as a nodal diameter trace, corresponding to the same resonance crossing as in Figure 1, refer to [9] for a description of this BTT data analysis method. Note that LSMF analysis of BTT measurements, because data sampling can occur only at discrete points of blade passing, FFT decomposition can also be conducted only at integer values in the range of $\bar{k} = -5 \dots +5$ (for the blade count = 11).

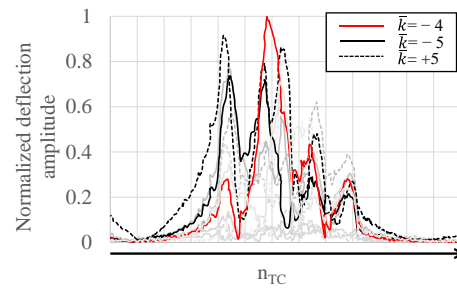


Figure 4. BTT nodal diameter trace output, normalized by the highest amplitude, resulted in $\bar{k} = -4$ (in the diagram, a trend of all \bar{k} values $-5 \dots +5$ is included but highlighted only \bar{k} values used for further discussion).

Note also that the author is intentionally avoiding the wording of nodal diameter (“ND”) and uses the symbol “ \bar{k} ” (circumferential mode index). The notion of “nodal diameter” provokes an image that a wave pattern is distributed equally around circumferences. However, as will be displayed later, in a mistuned structure, such an image by no means represents reality.

The highest amplitude is recorded in $\bar{k} = -4$, not in $\bar{k} = +5$. The rule about EO and excitable ND ($EO = 6, B = 11$) suggests that only $ND = +5$ mode must be excitable. This experimental result underlines that the notion of nodal diameter is inadequate for low EO resonances of a mistuned radial turbine.

Before presenting pulsation measurement results, let us recapture the frequency and wave number shift formulas in [2] when the frame of observation is transformed from rotating to stationary so that readers can follow further discussions easily.

$$\bar{k}l = \bar{k} + m \cdot B \tag{7}$$

$$\omega' = \omega + 2\pi \cdot (\bar{k} + m \cdot B) \cdot n_{TC} = 2\pi \cdot (EO + \bar{k} + m \cdot B) \cdot n_{TC} = 2\pi \cdot EO_{puls} \cdot n_{TC} \tag{8}$$

\bar{k} : circumferential mode index in the rotating frame of reference

$\bar{k}l$: circumferential mode index in the stational frame of reference

ω : frequency in the rotating frame of reference, i.e., blade vibration frequency

ω' : frequency in the stational frame of reference

EO_{puls} : observed engine order by the pulsation sensor (stationary frame of reference)

Recall the previous discussion, where the $m = +1$ mode will be dominant at the resonance condition of the first flap mode along $EO = 6$, depending on the circumferential mode index \bar{k} , a pulsation sensor detects the sound radiation at a different frequency or EO. If $\bar{k} = -4$ then $EO_{puls} = 6 - 4 + 11 = 13$. Consequently $\bar{k} = -5$ yields $EO_{puls} = 12$, and $\bar{k} = +5$ to $EO_{puls} = 22$, or 11 (coincides with BPFs).

Figure 5C displays the same trend, which is already presented in [1], but with additional information on individual blade trends. The pulsation amplitude trend along $EO_{puls} = 13$, obtained by FFT and order tracking analysis, matches almost perfectly the BTT $\bar{k} = -4$ trace trend. Around the speed range where the $\bar{k} = -4$ amplitude peak arises, the blade vibration amplitudes of Blades 5 and 6 or 7 and 8 were at comparable levels, and the IBPA between the set of Blades 5 and 6 or 7 and 8 met the prescribed value indeed for $\bar{k} = -4$, i.e., 131° , refer to Figure 5B. If the IBPA values lie within the given y-axis “range” (115–147 degrees), the peak amplitude of FFT decomposition corresponds to the energy contribution of $\bar{k} = -4$.

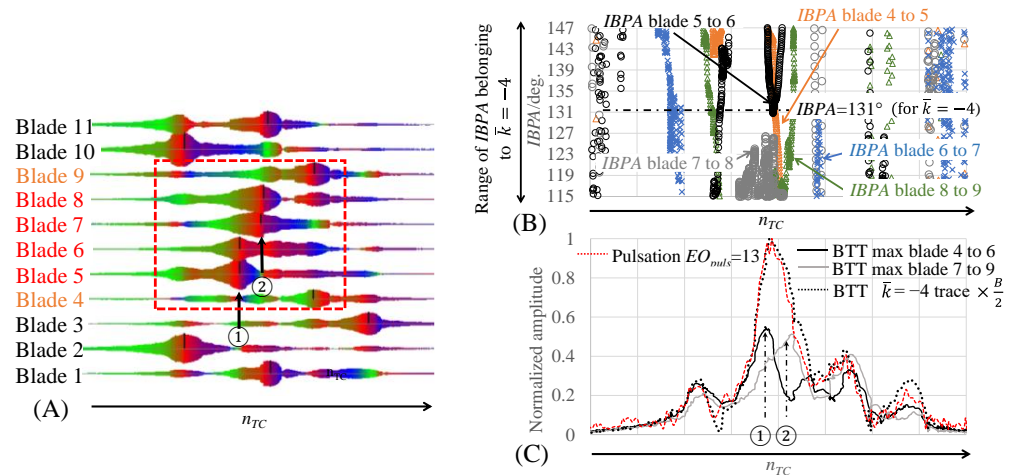


Figure 5. Comparison between BTT individual and $\bar{k} = -4$ traces with pulsation $EO_{puls} = 13$ order tracking result focusing on the behavior of Blades 4–9 (first flap mode along $EO=6$). (A) overall blade response; color indicates vibration phase transition. (B) selected *IBPA* trends over turbocharger revolution speed focusing on the *IBPA* range for $\bar{k} = -4$. (C) $\bar{k} = -4$ blade vibration mode amplitude trend overlaid with measured pulsation amplitude trend along $EO_{puls}=13$. The ① and ② highlight resonance crossing point of blade 5 and 6 or 7 and 8, respectively.

As demonstrated in Figure 5C, the main peak of the BTT $\bar{k} = -4$ traces can be reconstructed only by the trends of Blade pairs 5 and 6 and 7 and 8. The contributions of other blades are practically negligible.

Interestingly, around the main peak, *IBPA* values between 6 and 7—refer to the blue cross symbol in Figure 5B—do not lie in the $\bar{k} = -4$ range. Instead, they are placed in the range for $\bar{k} = +5$. In addition, especially at the resonance point of Blades 5 and 6—see the indication of ① in Figure 5A—the neighboring Blade 4 does not vibrate remarkably.

From the theoretical discussions in the previous chapters, it can be presumed that such sector-wise varying *IBPA*s or vibration amplitudes will influence sound radiation and interference characteristics in the downstream direction. To evaluate these presumptions, further investigations deploying computational fluid dynamics, as conducted by [10], would be desirable.

Figure 6 depicts the same kind of analysis as in Figure 5 but for the $\bar{k} = -5$ mode, proving that blade vibration detection using a pulsation sensor will also work well with another rather minor \bar{k} mode. The recorded pulsation peak amplitude along $EO_{puls} = 12$ was approximately 1/3 of that in $EO_{puls} = 13$. However, so far, the purpose of the method is condition-based monitoring, the monitoring will also work when pulsation signals along $EO_{puls} = 12$ are tracked. Compared to the case of $\bar{k} = -4$, the composition of contributing blades is more involved and will not be discussed further.

Finally, Figure 7 depicts the same kind of analysis as in Figure 5, but for the $\bar{k} = +5$ mode. Remember that the $\bar{k} = +5$ mode corresponds to the excitable circumferential mode along $EO = 6$ with blade count 11, and the observed *EO* (i.e., EO_{puls}), as a synonym for frequency from the stator side, will coincide with the BPF and its harmonics.

In this case, due to interference with the BPF mode, the pulsation peaks originating from blade vibration go in the negative direction, but the trend itself represents well the $\bar{k} = +5$ mode as a “mirrored image.” The base level of the BPF increased roughly from 0.3 to 0.9 in the displayed speed range, while the negative peak amplitude due to blade vibration amounts to ca. 0.3–0.4. This finding—that the pulsation peak along $EO_{puls} = \text{BPFs}$ due to blade vibration can have a negative direction, and, as such, blade vibration can also be detected—opens further perspectives of application ranges for this method. The first flap mode resonance along $EO = 6$ discussed hereabove occurs around 70% of maximal revolution speed. Around maximal revolution speed, however, blade tip sweep speed nears sound velocity so that BPFs mode starts to propagate downstream undiminished.

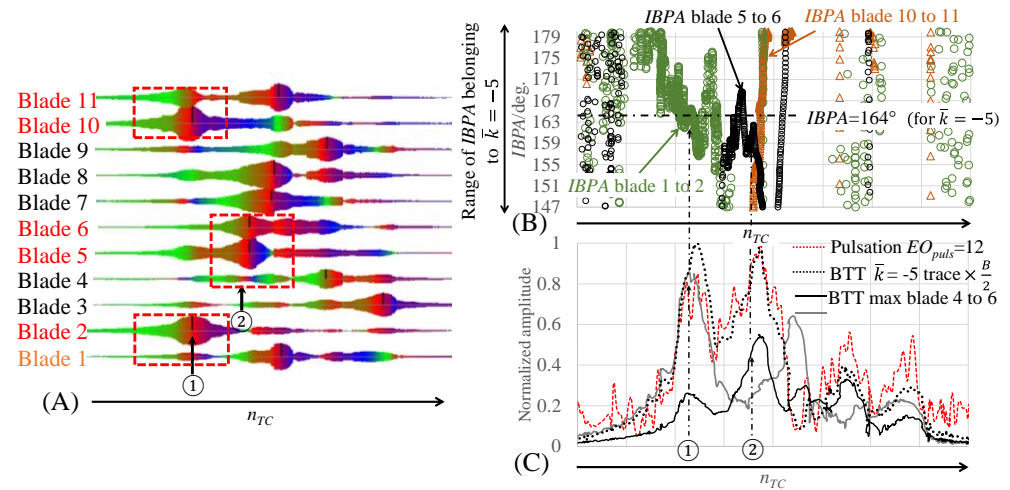


Figure 6. Comparison between BTT individual and $\bar{k} = -5$ traces with pulsation $EO_{puls} = 12$ order tracking result (first flap mode along $EO = 6$). (A) overall blade response; color indicates vibration phase transition. (B) selected IBPA trends over turbocharger revolution speed focusing on the IBPA range for $\bar{k} = -5$. (C) $\bar{k} = -5$ blade vibration mode amplitude trend overlaid with measured pulsation amplitude trend along $EO_{puls} = 12$. The ① and ② highlight resonance crossing point of blade 2, 10 and 11 or 5 and 6, respectively.

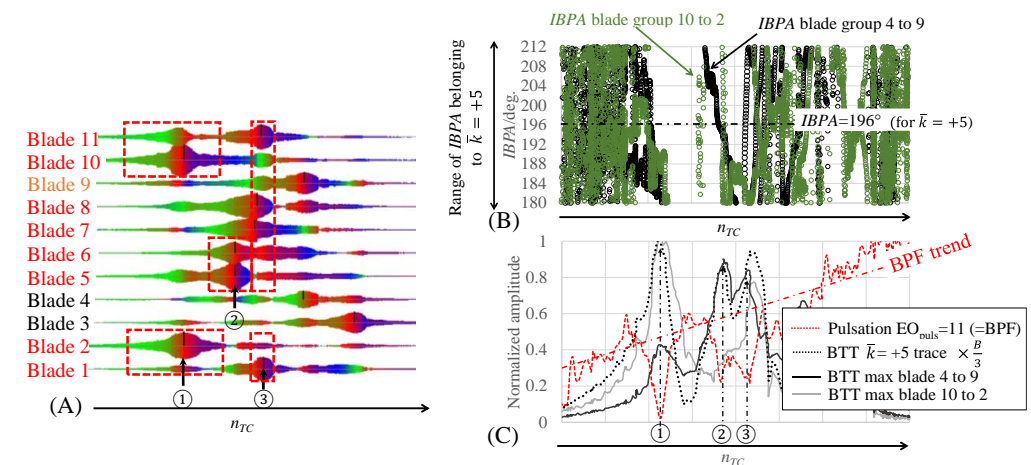


Figure 7. Comparison between BTT individual and $\bar{k} = +5$ traces with pulsation $EO_{puls} = 11$ order tracking result (first flap mode along $EO = 6$). (A) overall blade response; color indicates vibration phase transition. (B) selected IBPA trends over turbocharger revolution speed focusing on the IBPA range for $\bar{k} = +5$. (C) $\bar{k} = +5$ blade vibration mode amplitude trend overlaid with measured pulsation amplitude trend along $EO_{puls} = 11$. The ①, ② and ③ highlight resonance crossing point of blade 2, 10 and 11 or 5 and 6, or the others, respectively.

Figure 8 demonstrates that blade vibration detection will work with the method even when the blade tip speed is comparable to the speed of sound by analyzing another second mode resonance, which occurs along $EO = 8$. When the BPF mode starts to propagate undiminished, amplitudes will increase roughly fivefold, whereby the absolute pulsation amplitudes will exceed 100 mbar. The sharp drop of measured pulsation amplitude around the blade vibration resonance is, however, well distinguishable from gradual fluctuations originating from the BPF mode.

As demonstrated in Figure 8, by recognizing that pulsation peaks along BPFs can go in either a positive or negative direction relative to the base level, it can be claimed that this method can be applied for an entire (relevant) speed range to detect a potential danger of HCF failure.

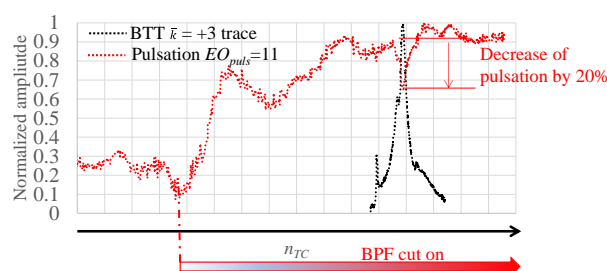


Figure 8. Comparison between BTT $\bar{k} = +3$ traces with pulsation $EO_{puls} = 11$ (= BPF) order tracking result for a second blade eigenmode resonance along $EO = 8$ occurring at around max. n_{TC} .

4. Conclusions

In this study, it has been proven that integral mode blade vibration detection using a single pulsation probe located away from the trailing edge is possible even with an actual mistuned structure and that the application range can be extended up to the maximum turbocharger revolution speed, where the blade tip speed approaches the speed of sound. Even if airborne acoustic waves are radiated from just a few sectors of a bladed rotor, the pulsation sensor can sense them. In a real mistuned structure, each sector (such as a blade pair) can vibrate with an arbitral *IBPA*, and the pulsation sensor on the stator side will sense these at different frequencies. Upon tracking several *EOs* neighboring the BPF, circumferential mode distribution, i.e., mistuning of the structure, can also be estimated in a certain extent. For condition-based monitoring, the fingerprint of the structure, i.e., pulsation peak amplitude distribution along several *EOs*, can be used to crosscheck if an event may really be related to an HCF danger.

Another advantage of this method is that the pulsation amplitude does not depend on frame size, so once an alarm level is defined in a convenient frame size within the standard HCF qualification process, it will be applicable to other frame sizes.

Funding: This research received no external funding.

Informed Consent Statement: Informed consent was obtained from all subjects involved in the study.

Data Availability Statement: Data cannot be shared because it relates to a product of Turbo Systems Switzerland Ltd.

Conflicts of Interest: The author declares no conflict of interests.

Nomenclature

| | |
|-------------|---|
| BPF | blade passing frequency |
| BTT | blade tip timing measurement |
| <i>EO</i> | excitation or engine order in rotating frame of reference (low <i>EO</i> refers up to $EO = 10$, excitation originates from geometrical irregularities of casing and/or nozzle ring) |
| EO_{puls} | excitation or engine order in stationary frame of reference (excitation order detected by pulsation sensor installed on stator side) |
| HCF | high cyclic fatigue |
| HFO | heavy fuel oil |
| <i>IBPA</i> | inter-blade phase angle |
| <i>ND</i> | nodal diameter (synonym for cyclic symmetrical mode) |
| LSMF | least square model fit used in BTT data analysis |
| NR | nozzle ring |
| <i>B</i> | turbine blade count |
| <i>M</i> | Mach number |
| <i>U</i> | axial bulk flow velocity |
| <i>V</i> | circumferential bulk flow velocity, $= 2 \cdot \pi \cdot r \cdot n_{TC}$ |

| | |
|----------------|---|
| W | relative bulk flow velocity |
| c_o | sound velocity |
| c_s | circumferential mode sweep velocity |
| i | natural number |
| k | integer in the range of $-\frac{B-1}{2} \leq k \leq \frac{B-1}{2}$ for odd number blade count |
| \bar{k} | circumferential mode index |
| m | airborne acoustic wave number between two blades |
| n_{TC} | rotor revolution frequency |
| r | outer radius at the blade trailing edge |
| ω | blade vibration frequency |
| $\bar{\alpha}$ | axial wave number defined by Equation (1) |
| $\bar{\beta}$ | global wave number between two blades defined by Equation (2) |

References

1. Ando, T. Pulsation and Vibration Measurement on Stator Side for Turbocharger Blade Vibration Monitoring. *Int. J. Turbomach. Propuls. Power* **2020**, *5*, 11. [CrossRef]
2. Mengle, V.G. Acoustic spectra and detection of vibrating rotor blades including row-to-row interference. In Proceedings of the AIAA 13th Aeroacoustics Conference, Tallahassee, FL, USA, 22–24 October 1990.
3. Kurkov, A.P. Flutter Spectral Measurements Using Stationary Pressure Transducers. *J. Eng. Power.* **1981**, *103*, 461–467. [CrossRef]
4. Kurkov, A.P. *Formulation of Blade Flutter Spectral Analyses in Stationary Reference Frame*; NASA TP-2296; NASA: Washington, DC, USA, 1984.
5. Tyler, J.M.; Sofrin, T.G. *Axial Flow Compressor Noise Studies*; S.A.E. International Transactions: Warrendale, PA, USA, 1962; Volume 70, pp. 309–332.
6. Zhao, F.; Nipkau, J.; Vahdati, M. Influence of Acoustic Reflection on Flutter Stability of an Embedded Blade Row. In Proceedings of the ETC11, Madrid, Spain, 23–27 March 2015.
7. Hanamura, Y.; Tanaka, H. A simplified Method to Measure Unsteady Forces Acting on the Vibrating Blades in Cascade. *Bull. JSME* **1980**, *23*, 880–887. [CrossRef]
8. Morse, P.M.; Ingard, K.U. *Theoretical Acoustics*. Chapter 11; Princeton University Press: Princeton, NJ, USA, 1987; ISBN 0-691-02401-4.
9. Agilis Measurement Systems. 2022. Available online: <https://agilismeasurementsystems.com/> (accessed on 7 January 2022).
10. Müller, T.R.; Vogt, D.M.; Vogel, K.; Phillipsen, B.A. Influence of Interflow Interaction on the Aerodynamic Damping of an Axial Turbine Stage. In Proceedings of the ASME Turbo Expo 2018, Lillestrøm, Norway, 11–15 June 2018.

Disclaimer/Publisher’s Note: The statements, opinions and data contained in all publications are solely those of the individual author(s) and contributor(s) and not of MDPI and/or the editor(s). MDPI and/or the editor(s) disclaim responsibility for any injury to people or property resulting from any ideas, methods, instructions or products referred to in the content.